Electrochimica Acta 492 (2024) 144344

Contents lists available at ScienceDirect

Electrochimica Acta

journal homepage: www.journals.elsevier.com/electrochimica-acta

New evidence on the electroprecipitation of ceria

Enrico Verlato [1,*], Nicola Comisso [1], Luca Mattarozzi [1], Marco Musiani [2], Lourdes Vázquez-Gómez [1]

Institute of Condensed Matter Chemistry and Technologies for Energy ICMATE - CNR, Corso Stati Uniti 4, Padova 35127, Italy

ARTICLE INFO

Keywords:
Alkalinization
Base generation
Nitrate reduction
Oxides
Porous layer

ABSTRACT

The electroprecipitation of ceria onto Ni electrodes from $Ce(NO_3)_3$ solutions has been studied by comparing deposits obtained with potentiostatic electrolysis of variable durations. The dependence on the deposition charge of (i) ceria layer thickness, (ii) apparent layer density, (iii) coverage of the Ni surface by CeO_2 and (iv) layer resistance was determined. These quantities were respectively assessed using (i) cross-sectional SEM images, (ii) gravimetric measurements, (iii) cyclic voltammetry in alkaline solution and (iv) electrochemical impedance spectroscopy. Experimental data showed that a porous low-density oxide precipitated initially, leaving a substantial part of the Ni electrode surface in direct contact with the electrolyte. During successive phases of the film growth, the formation of new solid material at the layer|solution interface was progressively replaced by its formation within the layers' pores and at the Ni|layer interface.

1. Introduction

Cathodic electroprecipitation is an effective and versatile method for the preparation of metal oxide/hydroxide layers onto conductive substrates. Depending on the selected metal oxide/hydroxide, applications in various fields, including corrosion protection, catalysis, fuel cells and solar energy conversion, have been proposed. In this method, which various authors have called in different ways (e.g., "cathodic generation of base" [1], cathodic electrolytic deposition [2] and electroprecipitation [3]), the oxide/hydroxide formation is triggered and sustained by a local pH increase at the cathode surface due to generation of hydroxide ions resulting from the reduction of species like NO_3^-, O_2, H_2O_2, H^+ or water. The mechanisms of the chemical reactions leading to the formation of oxide/hydroxide layers from the respective metal cations have been elucidated and many studies have addressed the morphology and crystalline structure of the deposited materials [3-6]. However, there have been few quantitative studies on the dependence of the deposit's density on experimental variables (Kong et al. [3] described the effect of deposition current on the density of $Ni(OH)_2$). Furthermore, to the best of our knowledge, there are no reports about the progressive coverage of the electrode surface by the solid oxide/-hydroxide material during film growth, i.e. about the progressive decrease of the electrode area in contact with the electrolyte and active in the reduction reactions mentioned above. In the present paper we present and discuss the results of experiments aimed at investigating these issues. The process chosen for this investigation was the electroprecipitation of ceria.

The cathodic electroprecipitation of ceria was pioneered by Switzer et al. [1,7-8] who used $Ce(NO_3)_3$ hexahydrate aqueous solutions as deposition baths. These authors clarified that the cathodic current density (j) determined the deposit morphology: powders were obtained at high j values ($j = 1$ A cm^{-2}) [7], films at low j values ($j < 5$ mA cm^{-2}) [8]. Their XRD analyses showed that the deposits consisted of CeO_2 and did not contain Ce(III) oxide. This means that, during the electroprecipitation, Ce(III) was oxidized to Ce(IV), although the process occurred at the cathode. This surprising result was explained by Aldykiewicz et al. [9] who, through X-ray absorption near edge structure (XANES) and rotating disc electrode (RDE) experiments, showed that dissolved oxygen favored the formation of Ce(IV)-rich films, especially under conditions that induced the 2-electron reduction of O_2 to H_2O_2 which, in turn, chemically oxidized Ce(III) to Ce(IV). Thermodynamic studies, aimed at calculating the pH required for the precipitation of Ce oxide [10], the speciation of Ce ions [11] and the Pourbaix diagrams for both the Ce-H_2O and the Ce–H_2O–H_2O_2 systems [12], supported the reaction mechanism proposed by Aldykiewicz et al. [9]. Electrochemical and chemical reactions involved in the electroprecipitation process are

* Corresponding author.
E-mail address: enrico.verlato@cnr.it (E. Verlato).
[1] ISE Active Member.
[2] ISE Honorary Member.

https://doi.org/10.1016/j.electacta.2024.144344
Received 25 January 2024; Received in revised form 11 April 2024; Accepted 27 April 2024
Available online 2 May 2024

reported at page 2 of the Supplementary Information.

A major motivation for the studies on the formation of ceria deposits was the hope that Ce ions might replace toxic and carcinogenic Cr(VI) in the production of anti-corrosion conversion coatings onto Al, Zn, mild steel and galvanized steel [13-16]. The significant inhibition efficiency of Ce salts was ascribed to the formation of Ce-rich coatings onto the cathodic areas, with a base generation mechanism essentially identical to that operating when a cathodic current was imposed [14]. With the aim of achieving thick and homogeneous coatings onto a variety of corrodible metal substrates, cathodic electroprecipitation of ceria was studied by various workers [17-24] who consistently observed the development of some defects and cracks when the coating thickness increased. Attempts to improve the coatings morphology and their anti-corrosion protection effectiveness included addition of H_2O_2 to the deposition baths [17,18], use of hydroalcoholic electrolytes [17,18] or use of additives [17].

Catalysis has been another major application domain of Ce oxide layers prepared through various synthetic approaches. CeO_2 is an effective catalyst for reactions like the oxidation of CO to CO_2 [25]. Acting as a co-catalyst in combination with noble metal nanoparticles [26,27], CeO_2 enhances their catalytic activity and protects them from agglomeration [28]. Structured CeO_2-noble metal catalysts are currently prepared using washcoating methods (e.g., see [29]). Our group has shown that quasi-core-shell Pt@CeO_2 nanoparticles, active in the catalytic low-temperature combustion of methanol, could be obtained by the sequential cathodic deposition of Pt and CeO_2 onto Fecralloy™ foams [30] and that Ru/Ce/Ni foam catalysts could be prepared by cathodic electroprecipitation of CeO_2 onto Ni foams to which Ru was added by impregnation, obtaining structured catalysts for the methanation of CO_2 [31]. We also showed that ceria films electroprecipitated onto boron-doped diamond cathodes enhanced the electrochemical reduction of CO_2 to formic acid at low overpotentials, with good faradaic efficiency [32].

2. Experimental

Two-compartment glass cells were used in all electrochemical experiments. Working and counter electrodes were positioned inside the main compartment; the reference electrodes (either a KCl saturated calomel electrode, SCE, or an Hg|HgO|0.5 M KOH electrode) were located in a side compartment connected to the main one through a Luggin capillary. All electrochemical experiments, i.e., potentiostatic electrolysis, linear/cyclic voltammetry and electrochemical impedance spectroscopy, were performed with an Autolab PGSTAT 302 N.

Gold screen printed electrodes (Au-SPE) with a 0.126 cm^2 geometric area, purchased from Metrohm, were used as working electrodes. Ahead of the electroprecipitation of ceria, they were submitted to Ni electrodeposition in a Watt's bath (1.126 M $Ni(SO_4)_2{\cdot}6H_2O$, 0.185 M $NiCl_2{\cdot}6H_2O$, 0.485 M H_3BO_3, pH 4.0, 25 °C) at a constant potential ($E = -1.0$ V), transferring in each case the same charge (10 C cm^{-2}) which induced the formation of continuous Ni layers, ca. 2 μm thick, which homogeneously coated the Au-SPE. SEM images of Ni electrodeposits are shown in Fig. S1.

Electroprecipitation of ceria onto Ni-plated Au SPEs was carried out under potentiostatic control (at −0.8, −1.0 or −1.2 V vs SCE), transferring different charges to obtain deposits of variable thickness. The deposition baths were 0.1 M $Ce(NO_3)_3{\cdot}6H_2O$ solutions (pH 4.5), gently stirred, kept at 25 °C with a thermostat, with a measured conductivity of ca. 22 mS cm^{-1}. They were frequently renewed (typically after transferring 8 C cm^{-2}).

The same electrodes and solutions were used in EIS experiments carried out in a potentiostatic mode, with a 10 mV rms ac signal, covering the selected frequency range (10 Hz – 10 kHz) with 8 points per decade. To monitor the possible formation of resistive layers, spectra were recorded, at the open circuit potential, before the electrolysis in Ce $(NO_3)_3$ solutions and after transferring increasing charges.

Samples for X-ray diffraction (XRD) analyses were obtained by drying the electrodeposits under vacuum at room temperature and detaching them from the electrodes. Some samples were thermally treated at 120 °C in air for 2 h. A Malvern Panalytical Empyrean diffractometer was employed in a Bragg-Brentano geometry (0.025°/step and 100 s/step). A Cu Kα source (40 kV and 40 mA) was used in all analyses. The peak positions were estimated with the instrumental fitting software Highscore Plus with the support of the standard patterns reported in the 2002 ICDD database.

The scanning electron microscopy (SEM) characterization of deposit morphology and thickness was performed with a FEI Quanta 200 FEG ESEM instrument, equipped with a field emission gun, operating at accelerating voltages between 10 and 25 kV. Both top views and cross-sectional images were recorded. In the latter case, ahead of Ni deposition, a deep linear scratch was made on the back face of the SPEs, opposite to the Au disc, to allow a controlled fracture of the electrodes bearing ceria deposits. The thickness of ceria films was measured at no less than 20 different positions and the obtained values were averaged.

With the aim of calculating the apparent density of the deposits, their mass was determined with a precision balance (Sartorius, Secura 125–1S, 0.01 mg precision) as the mass difference between the ceria-coated electrode and the same electrode ahead of the electroprecipitation. Before weighing, the ceria-coated electrodes removed from the $Ce(NO_3)_3$ solutions were carefully rinsed with deionized water, dried in a nitrogen stream and kept in a laboratory dessicator, under vacuum, during at least 12 h, until a constant mass was achieved.

The Ni-plated electrodes were submitted to cyclic voltammetry in deaerated 1 M KOH solution (scan rate 10 mV s^{-1}) and the redox charge exchanged in the $Ni(OH)_2$/NiOOH interconversion was measured. Indeed, such a charge has been shown to be proportional to the true surface area of nickel because both $Ni(OH)_2$ oxidation and NiOOH reduction are quasi-monolayer processes [33,34]. The same procedure was applied after deposition of ceria layers. The redox charges measured with the same Ni-plated Au SPE before and after deposition (Q^0 and Q^{CeO_2}, respectively) were used to compute θ_{CeO_2}, the percent ceria coverage at the deposit|Ni interface, according to Eq. (1),

$$\theta_{CeO_2} = 100\frac{Q^0 - Q^{CeO_2}}{Q^0} \quad (1)$$

θ_{CeO_2} was assumed to be identical to the percent decrease in the Ni area accessible to the electrolyte and electrochemically active during electrolysis. For the sake of comparison, Ni-plated Au SPEs were polarized at −1.2 V in 0.3 M $NaNO_3$ solution and then submitted to cyclic voltammetry in deaerated 1 M KOH solution.

3. Results and discussion

3.1. Electroprecipitation of ceria

There is extensive evidence that the cathodic electroprecipitation of ceria is a versatile process that can be realized on a variety of metal [1,2,7-9,17-24,35-37] and non-metal [38,39] electrodes, yielding deposits with comparable morphology. The reason why we selected Ni as a cathode material, among many other possibilities, is that its real surface area can be reliably assessed by cyclic voltammetry in alkaline media [33-34].

In the electroprecipitation experiments, we have preferred a potentiostatic control, rather than the more commonly used galvanostatic one, because it ensured that OH^- generation kept occurring during each electrolysis with constant contributions from the reduction of nitrate ions, the main process, and the reduction of H^+ and water, with limited generation of molecular hydrogen bubbles.

Fig. 1a shows a linear voltammogram recorded at low scan rate (5 mV s^{-1}) in a 0.1 M $Ce(NO_3)_3$ solution. Its shape agrees with those previously reported for the reduction of nitrate ions on Ni rotating disc

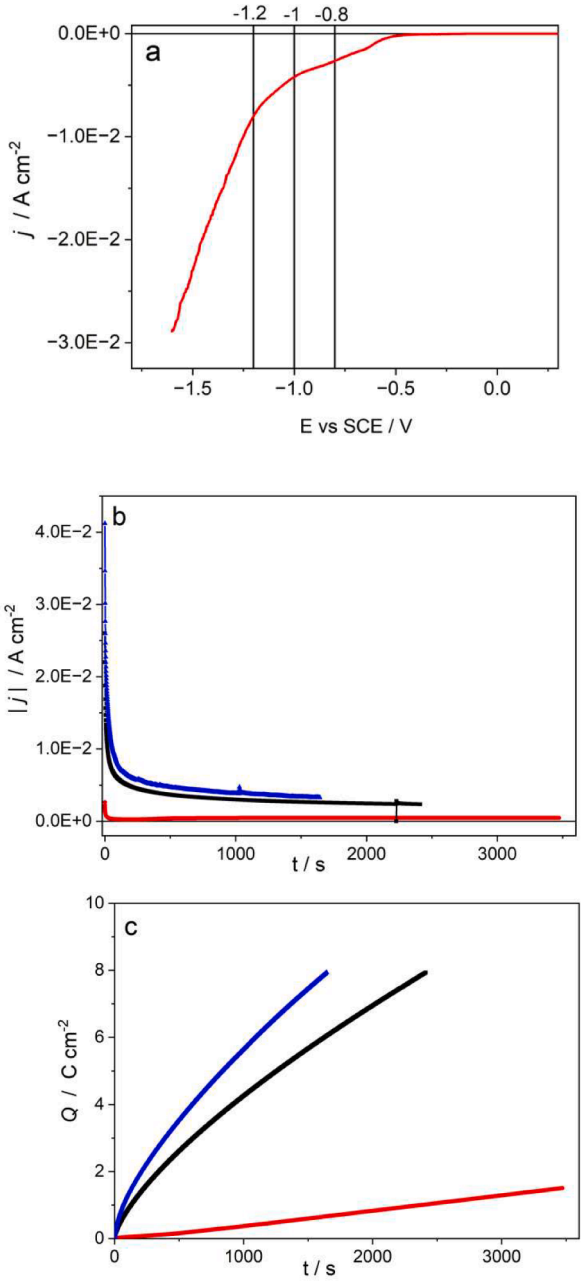

Fig. 1. Linear voltammograms recorded at a Ni-plated Au SPE in a 0.1 M Ce $(NO_3)_3$ solution (scan rate 5 mV s^{-1}) (a). Chronoamperometric (b) and chronocoulometric (c) curves recorded at $E = -0.8$ (red line), $E = -1.0$ (black line) and $E = -1.2$ V vs. SCE (blue line).

electrodes [40,41]. The vertical lines indicate the potential values that we used in potentiostatic electrolysis. Chronoamperometric and chronocoulometric curves recorded during such electrolyses are shown in Fig. 1b and 1c, respectively. Fig. 1b shows that, at each potential, the current density decreased with increasing electrolysis time, quite rapidly during an initial period of 1–2 min and then more slowly. A similar curve shape was reported by Li et al. [32], one of the few groups who deposited ceria at a constant cathode potential. Even at the most negative potential used in our investigation, the absolute value of the initial current density did not exceed 50 mA cm^{-2} and became lower than 10 mA cm^{-2} in about 1 min. Fig. 1c shows that the total charge transferred during the initial 1-minute period was at most 1 C cm^{-2}. Therefore, all the deposits studied in our investigation were mostly grown under conditions that approached those recommended by Switzer et al. [8] for the deposition of ceria films. Indeed, formation of powders not adhering to the electrode was never observed during electrolysis.

Deposition experiments were run at three cathode potential values: −0.8, −1.0 and −1.2 V (vs. SCE). The current measured at the least negative potential was much lower than in the other experiments and no significant deposition was observed. As shown in Fig. 1c, the deposition time necessary to transfer identical charges was ca. 50 % longer at −1.0 V than at −1.2 V. Although the most negative potential was likely to enhance H_2 formation, the electroprecipitated layers had only a few minor defects due to H_2 bubbles (see section 3.2 below). Therefore, we used a −1.2 V cathodic potential because it yielded deposits with high mechanical stability and very good adhesion to the Ni substrate.

Fig. 2 shows the X-ray diffractograms of deposits obtained at −1.2 V, either dried at room temperature or thermally treated at 120 °C in air. Reflections that could be attributed to either CeO_2 or $Ce(OH)_3$ were detected with the former sample, whereas the reflections due to CeO_2 dominated the diffractogram of the latter, in agreement with our

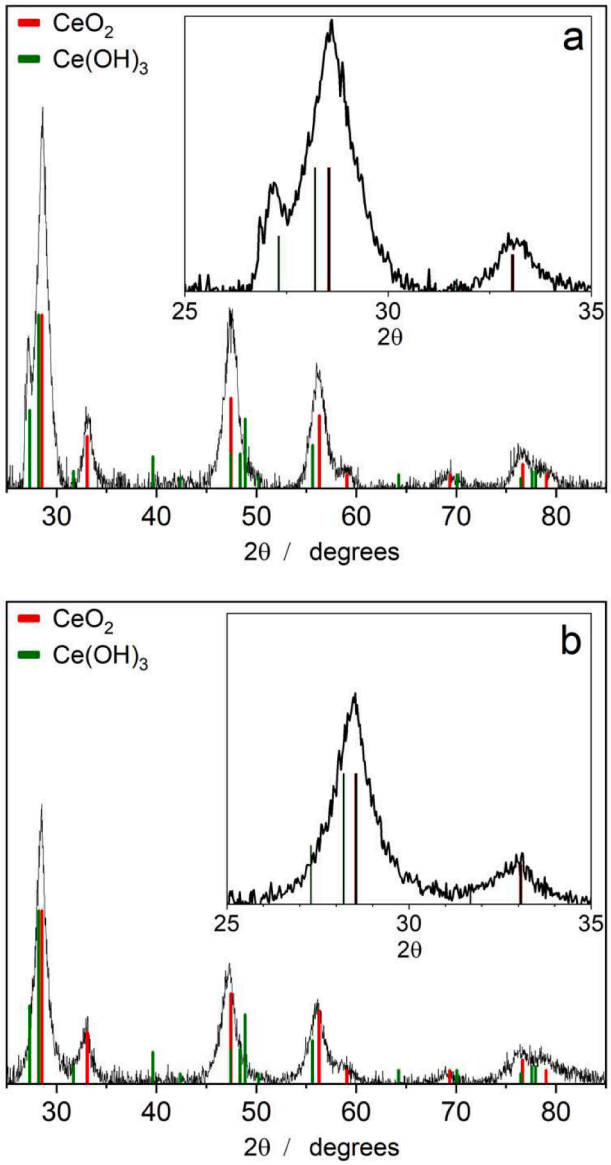

Fig. 2. X-ray diffractograms of deposits obtained at −1.2 V vs. SCE, either dried at room temperature (a) or thermally treated at 120 °C in air (b). The spectra are compared with the peaks respectively expected for CeO_2 (red) and $Ce(OH)_3$ (green) according to ICDD Card 34–0394 and ICDD Card 74–0665. The insets highlight the 25–35° region.

previous results [32]. Co-precipitation of CeO_2 and $Ce(OH)_3$ was observed by other groups who worked at low current density and/or in the absence of H_2O_2 [2,19,36]. Although the freshly precipitated layers did not consist of pure CeO_2, henceforth we will call them "ceria layers".

3.2. Thickness, apparent density and resistance of ceria layers

Ceria deposits of variable thickness were investigated using SEM. Fig. S2 in the Supplementary Information shows, as examples, the top views of some samples obtained with increasing deposition charges; it demonstrates that the film morphology remained essentially independent of the electrolysis duration.

Fig. 3 shows cross-sectional images of four deposits, each recorded with a magnification appropriate for a fairly accurate measurement of the film (average) thickness. Neither Fig. S2 nor Fig. 3 show significant defects that may be ascribed to H_2 gas bubbles incorporated in the deposits, however some defects sporadically appeared in other samples.

Fig. 4 (black circles) is a plot of the ceria layer thickness as a function of the deposition charge (the meaning of red squares in the same figure is discussed below). A quasi-linear thickness increase was observed for charges up to 5 C cm^{-2} (i.e. thicknesses up to ca. 50 μm), whereas, at larger charges, the film thickness seemed to reach a plateau, in agreement with the results of other authors who performed galvanostatic experiments, e.g. Zhithomirsky et al. [2] (who used chloride baths) and Pedraza et al. [21-23] (who used nitrate baths). A tendency of the deposit thickness to reach a limiting value was shown in [21].

The mass increase due to deposit formation was measured for each sample prepared with a deposition charge ≥ 2 C cm^{-2} (at lower charges, the accuracy in the determination of the deposit mass was too low). For each deposition charge, the deposit mass was divided by the respective deposit volume (computed from film thickness and electrode geometric area), to obtain apparent density values (ρ_{app}), plotted in Fig. 5 (black triangles) as a function of the deposition charge. The apparent density remained essentially constant, around 1 g cm^{-3}, for charges in the range 2–5 C cm^{-2} (a range where the thickness-charge dependence was quasi

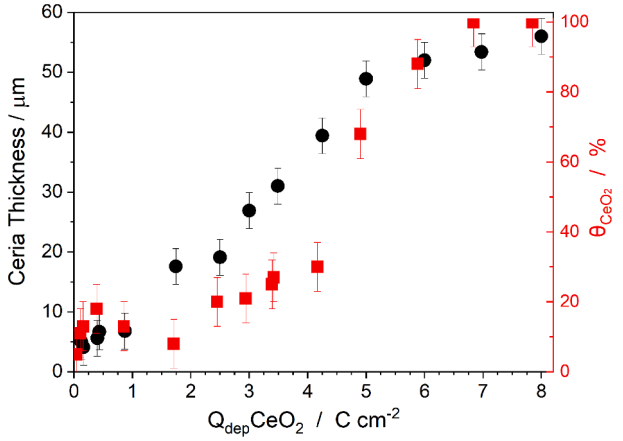

Fig. 4. Dependence of the ceria layer thickness (black circles) and ceria percent coverage of the Ni electrode area (red squares) on the deposition charge transferred during electrolysis at $E = -1.2$ V vs. SCE.

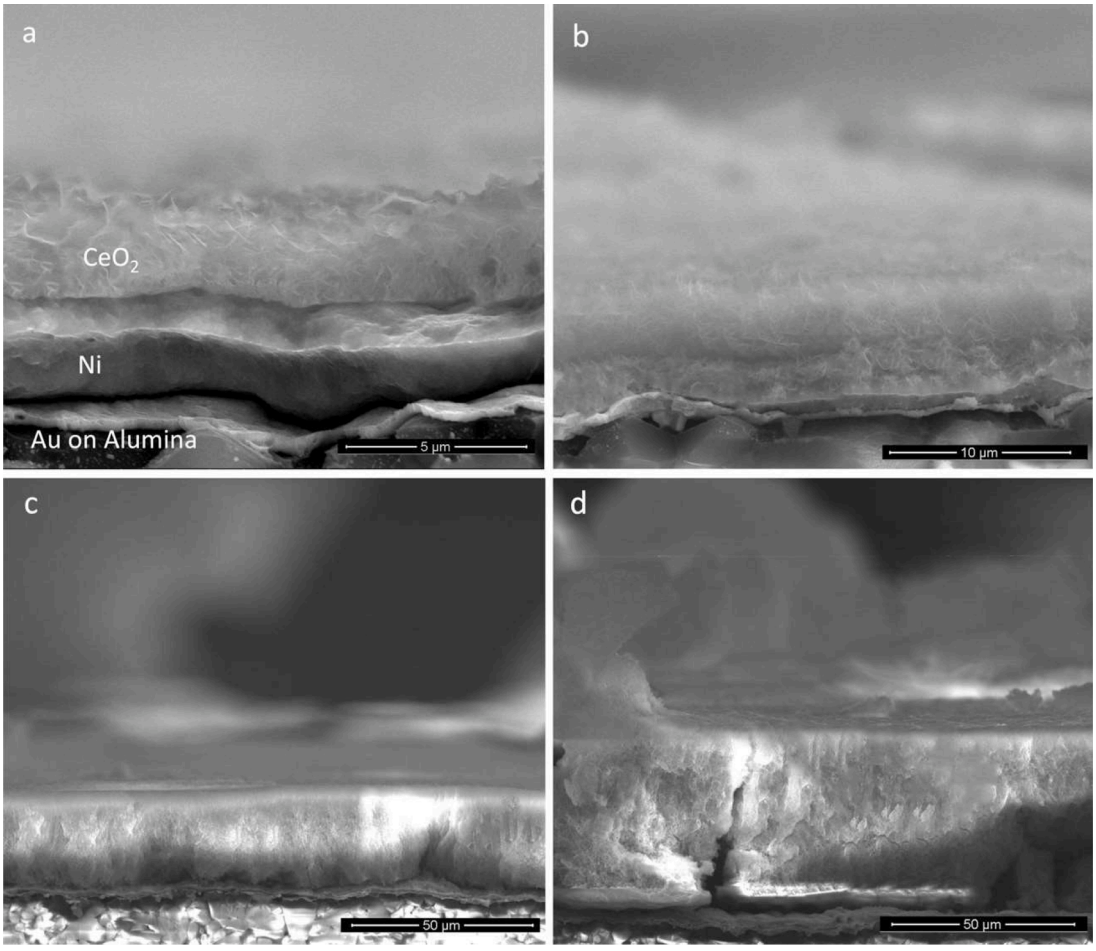

Fig. 3. Cross-sectional SEM images of four ceria layers obtained at $E = -1.2$ V vs. SCE, with variable deposition charges: 0.872 C cm^{-2} (a), 2.0 C cm^{-2} (b), 4.25 C cm^{-2} (c), 8.0 C cm^{-2} (d).

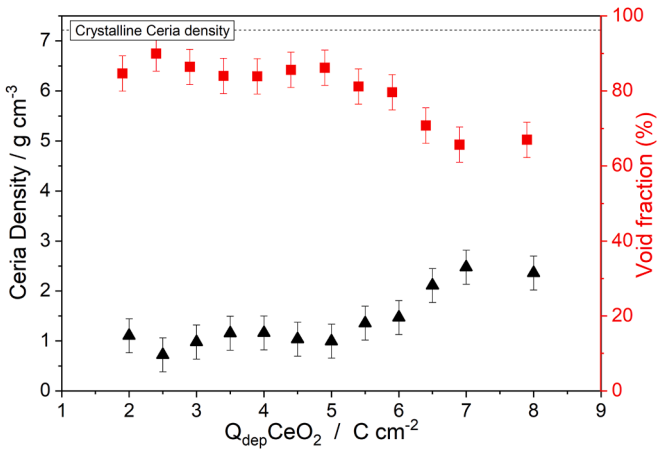

Fig. 5. Dependence of apparent density (black triangles, left ordinate axis) and void volume fraction (red circles, right ordinate axis) on the deposition charge transferred during electrolysis at $E = -1.2$ V vs. SCE. The density of crystalline CeO_2 is shown (dashed line).

linear), then progressively increased up to ca. 2.5 g cm^{-3}. Since the density of crystalline CeO_2 (ρ_{CeO2}) is 7.22 g cm^{-3}, the void volume fraction (V_{void}) of the deposits (red squares in Fig. 5), calculated according to Eq. (2)

$$V_{void} = 100\frac{\rho_{CeO2} - \rho_{app}}{\rho_{CeO2}} \quad (2)$$

was between 80 and 90 % at low deposition charges and decreased to ca. 60 % for the highest deposition charges used in our study. There is unanimous agreement among the authors who have studied ceria electroprecipitation that deposits formed in aqueous media are porous. Our apparent density data provides quantitative evidence on the extent of such porosity.

Kong et al. [3], who studied the electroprecipitation of $Ni(OH)_2$ from $Ni(NO_3)_2$ solutions using ellipsometry, measured density values in the range 1.25 to 1.5 g cm^{-3} for thin samples prepared at different current densities and reported that $Ni(OH)_2$ layers became less compact when prepared with larger currents. Similarly to our findings, the density values measured by Kong et al. [3] were lower than those of crystalline $Ni(OH)_2$ (reported by Chen et al. [42] to be in the range 2.5 – 2.8 g cm^{-3}).

Various authors have shown that ceria deposits became cracked when their thickness increased. In Fig. S3, low-magnification SEM images of two ceria layers with different thicknesses highlight the formation of some cracks which covered fractions of their area estimated to be ≤ 7 %. Thus, neglecting the presence of those cracks caused only a minor error in the calculation of the deposit's apparent density. Fig. S3 also shows that quasi-circular defect, due to H_2 bubbles, were rare, and that their number increased with deposit thickness.

Electrochemical impedance measurements were conducted to monitor the possible formation of resistive ceria layers that might influence the uncompensated ohmic drop and thus induce a progressive shift of the true cathode potential. The results are shown in Fig. S4a, where the high frequency limit of the real part of the impedance (average of at least five experiments) is plotted as a function of the deposition charge. Fig. S4b shows, the high-frequency range of the impedance measured before and after ceria deposition. No significantly increasing R_{hf} trend was observed (fluctuations were due in part to the not fully reproducible positioning of the working electrode in the cell) thus showing that the additional layer resistance was negligible as compared to the uncompensated electrolyte resistance. This result is coherent with the large porosity of all deposits and the presence of a rather concentrated electrolyte inside their pores.

3.3. Coverage of the Ni surface by electroprecipitated ceria

Considering their large void volume fraction (Fig. 5), each section of the ceria layer parallel to the electrode surface must be shared by the deposited solid material and the electrolyte that fills the layer's pores. If this holds at any depth along the film thickness, including at the Ni|layer interface, there must be areas of the Ni electrode occupied by solid material and other areas in direct contact with the electrolyte. To the best of our knowledge, no data has been published about the coverage of the electrode surface by electroprecipitated oxide/hydroxide materials and on its variation with the deposition charge. Therefore, we addressed this issue by immersing Ni-plated Au SPEs with different ceria loadings into deaerated 1.0 M KOH solution and submitting them to cyclic voltammetry. The results were then interpreted assuming that the Ni areas in contact with the electrolyte behaved like the bare electrode, i.e. they were the site of the $Ni(OH)_2$|NiOOH interconversion, but this reaction did not occur in the areas of the Ni surface in direct contact with solid ceria.

Fig. 6a-c shows cyclic voltammograms recorded, using either bare Ni electrodes (black traces) or ceria coated electrodes (red traces). The voltammograms compared in each part of this figure were obtained on the same individual electrode. The voltammograms recorded with bare Ni are not identical in parts a, b and c, because individual Ni-plated electrodes had different surface roughness (i.e. different true surface areas) caused by variations in the roughness of commercial Au SPEs.

Fig. 6a shows that the intensity of the redox peaks respectively due to $Ni(OH)_2$ oxidation (at 0.49 V) and NiOOH reduction (at 0.43 V) measured in the presence of a ceria film ca. 20 μm thick (deposition charge 2.0 C cm^{-2}) was only slightly lower than that measured with bare Ni. Then, in the presence of thicker deposits (Fig. 6b and 6c) the Ni $(OH)_2$/NiOOH redox peaks became progressively less intense and were just detectable for a 50 μm film.

The dependence of the ceria coverage, θ_{CeO_2}, calculated as described in the experimental section, on the deposition charge is shown in Fig. 4 (red squares). In contrast with the layer thickness, θ_{CeO_2} did not vary in a linear way. At low deposition charge (up to 0.3 C cm^{-2}), the coverage increased sharply from 0 to ca 15 %; then, there was only a minor increase for deposition charges up to 3 C cm^{-2}; finally, for deposition charges above 4 C cm^{-2}, the coverage increased markedly and approached 100 % when the deposition charge attained 7 C cm^{-2}.

Fig. 6 also shows that, in addition to quantitative variations in the intensity of the $Ni(OH)_2$/NiOOH peaks, ceria electroprecipitation induced qualitative changes in two distinct less positive potential ranges. At $E < -0.2$ V vs. Hg|HgO, we observed the appearance of a complex redox system, probably due to hydrogen adsorption/desorption onto/from Ni. Between −0.2 V and 0.3 V we measured an anodic current, essentially independent of potential and increasing with the ceria deposition charge, which we ascribe to oxidation of Ce(III) species in the deposited ceria layer to Ce(IV), in agreement with recent findings of Samantaray et al. [43]. As no corresponding cathodic process was observed, such oxidation appeared to be irreversible.

To check this hypothesis, we polarized Ni-plated Au SPEs in 0.3 M $NaNO_3$ solution at −1.2 V and then submitted those electrodes to cyclic voltammetry in 1.0 M KOH. Fig. 6d compares the results obtained after electrolysis in either $Ce(NO_3)_3$ or $NaNO_3$ solutions for the same electrolysis charge. In this figure, current data is presented as a dimensionless quantity obtained by dividing the measured current density (j) by the $Ni(OH)_2$ oxidation peak current ($j_{peak}^{Ni(OH)_2}$) measured, ahead of polarization, for each individual electrode. Fig. 6d shows that the anodic current between −0.2 V and 0.3 V was observed when a Ni-plated Au-SPE was polarized in $Ce(NO_3)_3$ but not after electrolysis in $NaNO_3$ solution, i.e. only when a ceria layer was deposited.

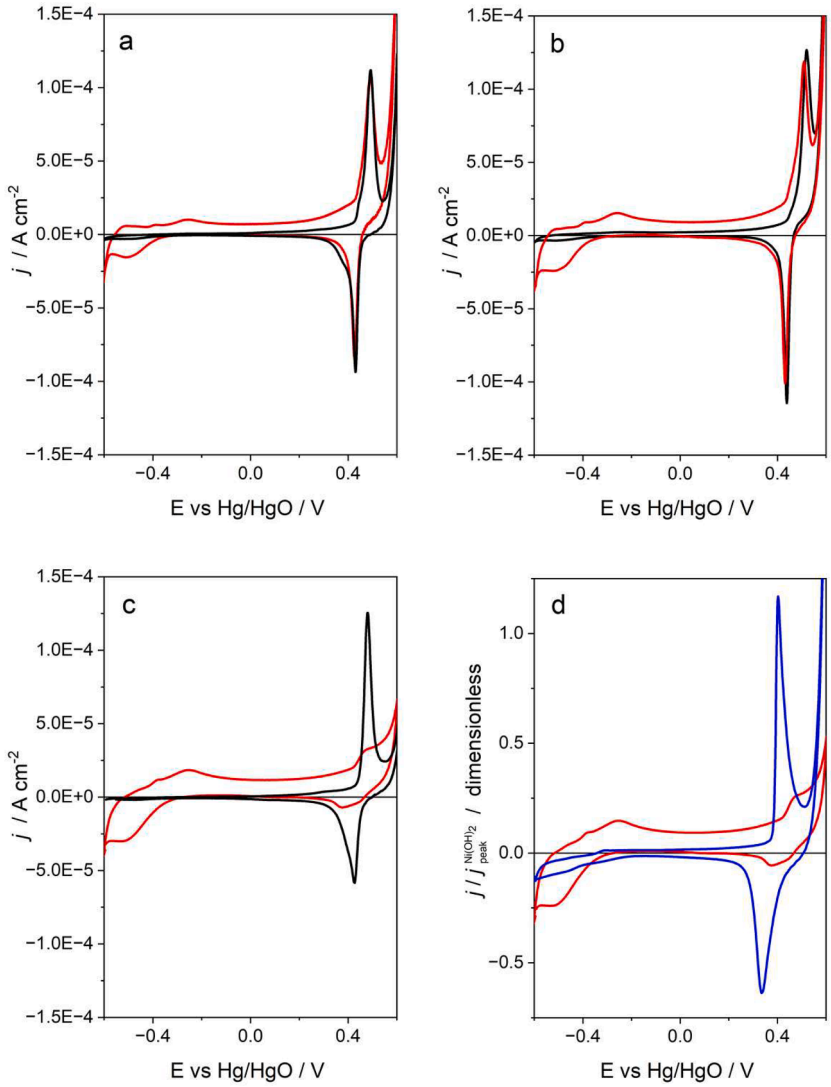

Fig. 6. (a) to (c): Cyclic voltammograms recorded in a 1.0 M KOH solution (scan rate 10 mV s^{-1}) with bare (black lines) and ceria-coated (red lines) Ni-plated Au SPEs, after electrolysis in a 0.1 M $Ce(NO_3)_3$ solution at −1.2 V vs. SCE, for the following deposition charges: (a) 2 C cm^{-2}, (b), 4.25 C cm^{-2}, (c) 6 C cm^{-2}. (d) Voltammograms obtained with Ni-plated Au SPEs respectively polarized in 0.1 M $Ce(NO_3)_3$ solution (red line) or 0.3 M $NaNO_3$ solution (blue line), both at −1.2 V vs. SCE with a 6 C cm^{-2} electrolysis charge. The ordinate axis shows the ratio between the measured current and the $Ni(OH)_2$ oxidation peak current at bare Ni.

3.4. Phases of the electroprecipitation of ceria

By taking simultaneously into account the chronoamperometric curves, the variation of thickness, apparent density and resistance of the deposited layers, and coverage of the Ni surface by solid oxide, one may recognize three successive phases in the electroprecipitation of ceria.

- Initial phase (deposition charge ≤ 0.5 C cm^{-2}). During the initial period, (i) the current density sharply decreases (ii) the deposit thickness increases with the deposition charge; (iii) the Ni electrode surface in direct contact with the electrolyte decreases only in a minor way. One may conclude that the nucleation and initial growth of a porous deposit, soaked by the electrolyte, occur during this period. The sharp decrease of current density is ascribed mainly to the depletion of nitrate ions and to the production of hydroxyl ions at the Ni/deposit interface, which both displaced the equilibrium potential to more negative values. The moderate decrease of the Ni area available for reduction reactions may have contributed to decreasing current, whereas the layer resistance was negligible. The deposit density could not be measured with our approach but, by extrapolating to low charges what observed in longer electrolysis for deposition charges up to 3 C cm^{-2}, one may speculate that it was ca. 1 g cm^{-3}.
- Intermediate phase (deposition charge between 0.5 and 4 C cm^{-2}). During this period, (i) the deposit thickness increases linearly with deposition charge; (ii) the deposit density remains essentially constant at ca. 1 g cm^{-3}; (iii) the coverage of the Ni surface undergoes only a moderate increase, roughly from 20 % to 30 %; (iv) the deposition current declines slowly and (v) the deposit resistance remains negligibly low. One may conclude that, during this period, the film growth occurs mainly at the layer|solution interface, thanks to the fast diffusion of the hydroxyl ions produced at the Ni surface, which maintains at that interface a pH value higher than the critical value for precipitation (ca. 8.5 according to [10]). Electron transport across the ceria layer and generation of hydroxyl ions due to reduction of nitrate at the layer|solution interface, which in principle might cause growth at that location, are very unlikely to occur due to the low electronic conductivity of ceria [44].
- Final phase (deposition charge between 4 and 8 C cm^{-2}). During this period, (i) the deposit thickness still increases but then approaches and attains a limiting value; (ii) the apparent deposit density increases significantly but remains far below that of crystalline ceria;

(iii) the coverage of the Ni surface almost attains 100 %; (iv) the deposition current declines slowly and the layer resistance remains much lower than the electrolyte resistance. One may conclude that, during this period, while the growth at the deposit/solution interface slows down and finally stops, the precipitation reaction continues to occur at the Ni|deposit interface and within the deposit's pores where, even with a diminished production of hydroxyl ions, the pH remains above the critical value and a sufficiently high Ce^{3+} ions concentration is maintained by diffusion from the solution bulk.

Some years ago, Murthy et al. [45] proposed a model for the electroprecipitation of thin $Ni(OH)_2$ films. Those authors assumed that the precipitation reaction occurred only at the $Ni(OH)_2$|solution interface. Our experimental evidence (i.e. increase in deposit density and progressive occupancy of the Ni surface) suggests that the model of Murthy et al., probably correct to describe their system, is not applicable to the electroprecipitation of ceria.

3.5. Catalytic activity at Ni|CeO_2 interfaces

The new experimental results described in this paper allow the rationalization of some observations described in a previous work of our group [31]. In that work, we prepared and tested structured catalysts for the conversion of CO_2 to CH_4, which consisted of Ni foams coated with electroprecipitated ceria, modified in some cases with Ru nanoparticles. The Ru-containing catalysts ensured CO_2 conversion close to equilibrium and selectivity for CH_4 close to 100 %. Catalysts without Ru nanoparticles were significantly less effective, as it could be anticipated, based on previous reports [46,47]. However, Fig. 7 (where selected data already reported in [31] are displayed) shows that, unexpectedly, their activity and selectivity markedly increased with the CeO_2 thickness. In our experiments [31], the CeO_2 deposition charges used in the preparation of the catalysts were at most 0.3 C cm^{-2}, i.e. in a range where ceria coverage of the Ni surface increased with loading. Significantly higher deposition charges were not used since thick coatings might have induced gas transport limitations. Since CeO_2 alone is unable to catalyze the methanation reaction, the reason for the enhanced catalysis at higher CeO_2 loading was tentatively ascribed to the formation of a larger number of interfacial Ni-CeO_2 sites in catalysts with thicker CeO_2 coatings. The coverage data reported above (Fig. 4, red squares) show the progressive increase of θ_{CeO_2} with the deposition charge and therefore supports that hypothesis.

4. Conclusion

Systematic experiments aimed at assessing the effect of deposition charge on the properties of electroprecipitated ceria layers gave the following results:

- the layer thickness increased in a quasi-linear way with the deposition charge, up to approaching a limiting value,
- the apparent density of the deposited material increased from ca. 1 to ca. 2.5, remaining much lower than that of crystalline CeO_2,
- the ceria coverage of the Ni surface grew quickly at low charges, remained essentially constant during the linear growth of the film thickness, and finally attained 100 %,
- throughout the deposition, the layer resistance remained too low to affect the ohmic drop.

These results suggested the initial deposition of a highly porous oxide/hydroxide material which was in direct contact with only a minor fraction of the underlying Ni surface. The electroprecipitation continued, sustained by the generation of hydroxyl ions at the bare Ni areas and their diffusion towards the electrolyte. For intermediate deposition charges, the precipitation of ceria occurred mainly at the layer|solution interface, without significant increase of the deposit density. At longer deposition time, with the decline of deposition current, hydroxyl ions were generated at lower rates and had to diffuse across thicker layers; the precipitation reaction progressively moved to the inner volume of the layers' pores, with a consequent density increase, and at the Ni|layer interface which became extensively blocked when the layer's thickness attained an upper limit [44].

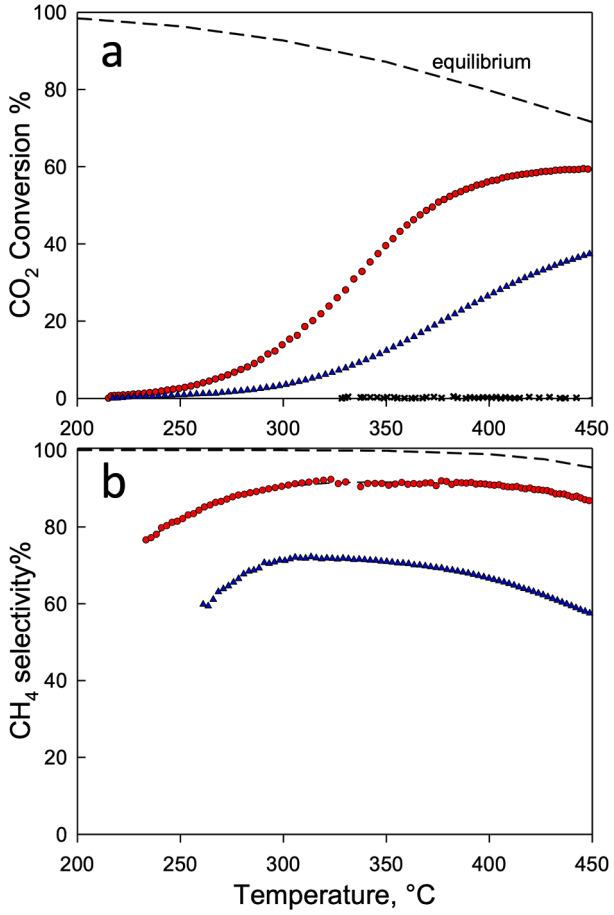

Fig. 7. Temperature dependence of CO_2 conversion (a) and CH_4 selectivity (b) during the hydrogenation of CO_2 over bare and CeO_2-coated Ni foam catalysts. Feed: $CO_2/H_2/N_2 = 1/4/5$. Dashed lines represent thermodynamic equilibrium. Ceria deposition charges were 0.1 C cm^{-2} (blue triangles) or 0.3 C cm^{-2} (red circles). Black crosses refer to bare Ni foam.

CRediT authorship contribution statement

Enrico Verlato: Writing – original draft, Supervision, Investigation, Formal analysis, Data curation, Conceptualization. **Nicola Comisso:** Writing – review & editing. **Luca Mattarozzi:** Writing – review & editing, Investigation. **Marco Musiani:** Writing – original draft, Supervision, Conceptualization. **Lourdes Vázquez-Gómez:** Writing – review & editing.

Declaration of competing interest

The authors declare that they have no known competing financial interests or personal relationships that could have appeared to influence the work reported in this paper.

Data availability

Data will be made available on request.

Acknowledgement

The authors thank Mr. Pierpaolo Caliaro for help in the analysis of SEM images to determine crack occupation, Mr. Paolo Tognana for equipment and software management and Dr. Stefano Cimino for useful discussions.

This research was partially funded by the European Union – Next-Generation EU from the Italian Ministry of Environment and Energy Security POR H2 AdP MMES/ENEA with involvement of CNR and RSE, PNRR - Mission 2, Component 2, Investment 3.5 "Ricerca e sviluppo sull'idrogeno".

Supplementary materials

Supplementary material associated with this article can be found, in the online version, at doi:10.1016/j.electacta.2024.144344.

References

[1] J.A. Switzer, Electrochemical synthesis of ceramical films and powders, Am. Ceram. Soc. Bull. 66 (1987) 1521–1524.
[2] I. Zhitomirsky, A. Petric, Electrolytic and electrophoretic deposition of CeO_2 films, Mater. Lett. 40 (1999) 263–268.
[3] F. Kong, R. Kostecki, F. McLarnon, In situ ellipsometric study of the electroprecipitation of nickel hydroxide films, J. Electrochem. Soc. 145 (1998) 1174–1178.
[4] E.A. McNally, I. Zhitomirsky, D.S. Wilkinson, Cathodic electrodeposition of cobalt oxide films using polyelectrolytes, Materials Chemistry and Physics 91 (2005) 391–398.
[5] L. Gal-Or, I. Silberman, R. Chaim, Electrolytic $Zr0_2$ Coatings, J. Electrochem. Soc. 138 (1991) 1939–1942.
[6] S. Peulon, D. Lincot, Mechanistic Study of Cathodic Electrodeposition of Zinc Oxide and Zinc Hydroxychloride Films from Oxygenated Aqueous Zinc Chloride Solutions, J. Electrochem. Soc. 145 (1998) 864–874.
[7] Y.C. Zhou, J.A. Switzer, Electrochemical Synthesis and Sintering of Nanocrystalline Cerium(IV) Oxide Powders, J. Am. Ceram. Soc. 78 (1994) 981–985.
[8] Y. Zhou, J.A. Switzer, Growth of cerium (IV) oxide films by the electrochemical generation of base method, J. Alloys Compd. 237 (1996) 1–5.
[9] Jr. A.J. Aldykiewicz, A.J. Davenport, H.S. Isaacs, Studies of the Formation of Cerium-Rich Protective Films Using X-Ray Absorption Near-Edge Spectroscopy and Rotating Disk Electrode Methods J. Electrochem. Soc. 143 (1996) 147–154.
[10] M.A. Arenas, J.J. de Damborenea, Growth mechanisms of cerium layers on galvanised steel, Electrochim. Acta 48 (2003) 3693–3698.
[11] B. Bouchaud, J. Balmain, G. Bonnet, F. Pedraza, pH-distribution of cerium species in aqueous systems, J. Rare Earths 30 (2012) 559–562.
[12] P. Yu, S.A. Hayes, T.J. O'Keefe, M.J. O'Keefe, J.O. Stoffer, The Phase Stability of Cerium Species in Aqueous Systems II. The Ce(III/IV)-H_2O-H_2O_2/O_2 Systems. Equilibrium Considerations and Pourbaix Diagram Calculations, J. Electrochem. Soc. 153 (2006) C74–C79.
[13] B.R.W. Hinton, Corrosion inhibition with rare earth metal salts, J. Alloys Compd. 180 (1992) 15–25.
[14] Jr A.J. Aldykewicz, H.S. Isaacs, A.J. Davenport, The investigation of cerium as a cathodic inhibitor for aluminum-copper alloys, J. Electrochem. Soc. 142 (1995) 3342–3350.
[15] M.F. Montemor, A.M. Simoes, M.G.S. Ferreira, Composition and behaviour of cerium films on galvanised steel, Prog. Org. Coat. 43 (2001) 274–281.
[16] M.F. Montemor, A.M. Simoes, M.G.S. Ferreira, Composition and corrosion behaviour of galvanised steel treated with rare-earth salts: the effect of the cation, Prog. Org. Coat. 44 (2002) 111–120.
[17] I. Zhitomirsky, A. Petric, Electrochemical deposition of ceria and doped ceria films, Ceram. Int. 27 (2001) 149–155.
[18] J. Creus, F. Brezault, C. Rebere, M. Gadouleau, Synthesis and characterisation of thin cerium oxide coatings elaborated by cathodic electrolytic deposition on steel substrate, Surf. Coat. Tech. 200 (2006) 4636–4645.
[19] Y. Hamlaoui, F. Pedraza, L. Tifouti, Investigation of electrodeposited cerium oxide based films on carbon steel and of the induced formation of carbonated green rusts, Corros. Sci. 50 (2008) 2182–2188.
[20] Y. Hamlaoui, F. Pedraza, C. Remazeilles, S. Cohendoz, C. Rébéré, L. Tifouti, J. Creus, Cathodic electrodeposition of cerium-based oxides on carbon steel from concentrated cerium nitrate solutions. Part I. Electrochemical and analytical characterisation, Mater. Chem. Phys. 113 (2009) 650–657.
[21] Y. Hamlaoui, L. Tifouti, C. Remazeilles, F. Pedraza, Cathodic electrodeposition of cerium based oxides on carbon steel from concentrated cerium nitrate. Part II: Influence of electrodeposition parameters and of the addition of PEG, Mater. Chem. Phys. 120 (2010) 172–180.
[22] B. Bouchaud, J. Balmain, G. Bonnet, F. Pedraza, Optimizing structural and compositional properties of electrodeposited ceria coatings for enhanced oxidation resistance of a nickel-based superalloy, Appl. Surf. Sci. 268 (2013) 218–224.
[23] B. Bouchaud, J. Balmain, G. Bonnet, F. Pedraza, Correlations between electrochemical mechanisms and growth of ceria based coatings onto nickel substrates, Electrochim. Acta 88 (2013) 798–806.
[24] D. Stoychev, Corrosion protective ability of electrodeposited ceria layers, J. Solid State Electr. 17 (2013) 497–509.
[25] A. Trovarelli, Catalytic properties of ceria and CeO_2-containing materials, Catal. Rev. 38 (1996) 439–520.
[26] M. Fernandez-Garcia, A. Martinez-Arias, L.N. Salamanca, J.M. Coronado, J. A. Anderson, J.C. Conesa, J. Soria, Influence of ceria on Pd activity for the CO + O_2 reaction, J. Catal. 187 (1999) 474–485.
[27] H.S. Gandhi, G.W. Graham, R.W. McCabe, Automotive exhaust catalysis, J. Catal. 216 (2003) 433–442.
[28] S. Lee, J. Seo, W. Jung, Sintering-resistant Pt@CeO_2 nanoparticles for high temperature oxidation catalysis, Nanoscale 8 (2016) 10219–10228.
[29] P. Fornasiero, T. Montini, M. Graziani, S. Zilio, M. Succi, Development of functionalized Fe–Al–Cr alloy fibers as innovative catalytic oxidation devices, Catal. Today 137 (2008) 475–482.
[30] E. Verlato, S. Barison, S. Cimino, L. Lisi, G. Mancino, M. Musiani, F. Paolucci, Electrochemical preparation of nanostructured Pt-CeO_2 catalysts on Fe-Cr-Al alloy foams for the low-temperature combustion of methanol, Chem. Eng. J. 317 (2017) 551–560.
[31] S. Cimino, E.M. Cepollaro, L. Lisi, S. Fasolin, M. Musiani, L. Vázquez-Gómez, Ru/Ce/Ni metal foams as structured catalysts for the methanation of CO_2, Catalysts 11 (2021) 13.
[32] E. Verlato, S. Barison, Y. Einaga, S. Fasolin, M. Musiani, L. Nasi, K. Natsui, F. Paolucci, G. Valenti, CO_2 reduction to formic acid at low overpotential on BDD electrodes modified with nanostructured CeO_2, J. Mat. Chem. A 7 (2019) 17896–17905.
[33] M.A. Sattar, B.E. Conway, Electrochemistry of the nickel-oxide electrode-VI. Surface oxidation of nickel anodes in alkaline solution, Electrochim. Acta 14 (1969) 695–710.
[34] R.S. Schrebler Guzman, J.R. Vilche, A.J. Arvia, Rate processes related to the hydrated nickel hydroxide electrode in alkaline solutions, J. Electrochem. Soc. 125 (1978) 1578–1587.
[35] F.B. Li, R.C. Newman, G.E. Thompson, In situ atomic force microscopy studies of electrodeposition mechanism of cerium oxide films: nucleation and growth out of a gel mass precursor, Electrochim. Acta 42 (1997) 2455–2464.
[36] P. Bocchetta, M. Santamaria, F. Di Quarto, Cerium oxyhydroxide nanowire growth via electrogeneration of base in nonaqueous electrolytes, Electrochem. Solid-State Lett. 11 (2008) K93–K97.
[37] Yuting Luo, Juan Li, Jie Zhu, Ye Zhao, Xuefeng Gao, Fabrication of Condensate Microdrop Self-Propelling Porous Films of Cerium Oxide Nanoparticles on Copper Surfaces, Angew. Chem. Int. Ed. 54 (2015) 4876–4879.
[38] V. Fernandes, J.J. Klein, W.H. Schreiner, N. Mattoso, D.H. Mosca, Electrodeposition of nanocrystalline CeO_2 on Si(001), J. Electrochem. Soc. 156 (2009) E199–E204.
[39] F. Faisal, A. Toghan, I. Khalakhan, M. Vorokhta, V. Matolin, J. Libuda, Characterization of thin CeO_2 films electrochemically deposited on HOPG, App. Surf. Sci. 350 (2015) 142–148.
[40] L. Mattarozzi, S. Cattarin, N. Comisso, P. Guerriero, M. Musiani, L. Vázquez-Gómez, E. Verlato, Electrochemical reduction of nitrate and nitrite in alkaline media at Cu-Ni alloy electrodes, Electrochim. Acta. 89 (2013) 488–496.
[41] L. Mattarozzi, S. Cattarin, N. Comisso, M. Musiani, L. Vázquez-Gómez, E. Verlato, Electrodeposition of Ni-Rh alloys and their use as cathodes for nitrate reduction in alkaline solutions, ChemElectroChem 10 (2023) e202201122.
[42] R.R. Chen, Y. Mo, D.A. Scherson, In situ atomic force microscopy imaging of electroprecipitated nickel hdrous oxide films in alkaline electrolytes, Langmuir 10 (1994) 3933–3936.
[43] Y. Samantaray, D.J. Martin, R.G. Agarwal, N.J. Gibson, J.M. Mayer, Proton-coupled electron transfer of cerium oxide nanoparticle thin-film electrodes, J. Phys. Chem. C 127 (2023) 4015–4020.
[44] Y.M. Chiang, E.B. Lavik, I. Kosacki, H.L. Tuller, Nonstoichiometry and electrical conductivity of nanocrystalline CeO_{2-x}, J. Electroceram. 1 (1997) 7–14.
[45] M. Murthy, G.S. Nagarajan, J.W. Weidner, J.W. Van Zee, A model for the galvanostatic deposition of nickel hydroxide, J. Electrochem. Soc. 143 (1996) 2319–2327.
[46] J. Artz, T.E. Müller, K. Thenert, J. Kleinekorte, R. Meys, A. Sternberg, A. Bardow, W. Leitner, Sustainable conversion of carbon dioxide: an integrated review of catalysis and life cycle assessment, Chem. Rev. 118 (2018) 434–504.
[47] H.T.T. Nguyen, Y. Kumabe, S. Ueda, K. Kan, M. Ohtani, K. Kobiro, Highly durable Ru catalysts supported on CeO_2 nanocomposites for CO_2 methanation, Appl. Catal. A Gen. 577 (2019) 35–43.